# Substrate Dependence of Conformational Changes in the RNA-Binding Domain of Tristetraprolin Assessed by Fluorescence Spectroscopy of Tryptophan Mutants†

Brandy Y. Brewer,‡ Jeff D. Ballin,‡ Elizabeth J. Fialcowitz-White,‡ Perry J. Blackshear,§ and Gerald M. Wilson*,‡

*Department of Biochemistry and Molecular Biology and Marlene and Stewart Greenebaum Cancer Center, University of Maryland School of Medicine, Baltimore, Maryland 21201, and Laboratory of Signal Transduction and Office of Clinical Research, National Institute of Environmental Health Sciences, National Institutes of Health, Department of Health and Human Services, Research Triangle Park, North Carolina 27709*

*Received June 30, 2006; Revised Manuscript Received September 12, 2006*

ABSTRACT: Association of tristetraprolin (TTP) with mRNAs containing selected AU-rich mRNA-destabilizing elements (AREs) initiates rapid cytoplasmic degradation of these transcripts. The RNA-binding activity of TTP is mediated by an internal tandem zinc finger domain that preferentially recognizes U-rich RNA ligands containing adjacent UUAU half-sites and is accompanied by conformational changes within the peptide. Here, we have used analogues of the TTP RNA-binding domain containing specific tryptophan substitutions to probe the $Zn^{2+}$ and RNA substrate dependence of conformational events within individual zinc fingers. Fluorescence methods demonstrate that the N-terminal, but not C-terminal, zinc finger domain adopts a stably folded conformation in the presence of $Zn^{2+}$. Denaturant titrations suggest that both the N- and C-terminal zinc fingers exhibit limited structural heterogeneity in the absence of RNA substrates, although this is more pronounced for the C-terminal finger. Binding to a cognate ARE substrate induced significant conformational changes within each zinc finger, which also included increased resistance to chemical denaturation. Studies with mutant ARE ligands revealed that a single UUAU half-site was sufficient to induce structural modulation of the N-terminal finger. However, RNA-dependent folding of the C-terminal zinc finger was only observed in the presence of tandem UUAU half-sites, suggesting that the conformation of this domain is linked not only to RNA substrate recognition but also to the ligand occupancy and/or conformational status of the N-terminal finger. Coupled with previous structural and thermodynamic analyses, these data provide a mechanistic framework for discrimination of RNA substrates involving ligand-dependent conformational adaptation of both zinc fingers within the TTP RNA-binding domain.

In mammals, many mRNAs that encode proteins contributing to the control of cell proliferation, differentiation, apoptosis, and intercell communication are inherently unstable. This property limits the cytoplasmic concentration of these mRNAs, and hence their potential for translation, but also permits new steady-state mRNA levels to be attained rapidly following changes in the synthetic rate (*1*, *2*). The degradation of many labile mRNAs is directed by the presence of AU-rich elements (AREs)[1] within their 3′-untranslated regions (3′UTRs). AREs constitute a broad family of mRNA-destabilizing sequences ranging from approximately 40 to 150 bases in length and frequently containing one or more AUUUA motifs within a U-rich tract (*3*−*5*). While the sequences of these *cis*-acting elements show remarkable diversity across the mRNA population, AREs from specific mRNAs are often highly conserved across species (*6*−*8*), implying that variations in ARE character may facilitate gene-specific control of mRNA decay kinetics. mRNA turnover directed by AREs is initiated by rapid 3′→5′ exonuclease digestion of the poly(A) tail (*9*, *10*), followed by 5′-decapping and decay of the mRNA body, which may involve both 3′→5′ and 5′→3′ exoribonucleolytic components (*11*−*16*).

Control of mRNA decay through AREs is mediated by the association of cellular *trans*-acting factors. To date, upward of 20 distinct proteins (*17*, *18*) and one microRNA (*19*) targeting AU-rich RNA sequences have been identified, although functional significance has been ascribed to only a small subset of these interactions. The ARE-binding factor tristetraprolin (TTP; also known as TIS11 and Nup475) is the prototype of a family of tandem CCCH zinc finger proteins (*20*) and promotes accelerated mRNA turnover in cells (*10*, *21*), possibly via direct recruitment of RNA catabolic activities. Recent data indicate that TTP can interact with numerous mRNA-degrading factors, including some responsible for 3′→5′ deadenylation and decay, 5′-decapping, and 5′→3′ exonuclease activities (*11*, *13*, *22*). TTP may also target mRNAs for degradation via an RNA interference-based mechanism, by enhancing the association

† This work was supported by NIH/NCI Grant CA102428 and a Scientist Development Grant from the American Heart Association (to G.M.W.).

* To whom correspondence should be addressed. Telephone: (410) 706-8904. Fax: (410) 706-8297. E-mail: gwils001@umaryland.edu.

‡ University of Maryland School of Medicine.

§ National Institute of Environmental Health Sciences.

[1] Abbreviations: ARE, AU-rich element; GMSA, gel mobility shift assay; GnHCl, guanidine hydrochloride; HSQC, heteronuclear single-quantum coherence; TTP, tristetraprolin; UTR, untranslated region.

10.1021/bi061320j CCC: $33.50 
Published on Web 10/31/2006

of microRNA miR16 with ARE-containing mRNA substrates (*19*). However, unlike some other ARE-binding proteins that readily bind diverse populations of U-rich RNA sequences (*8*, *23*−*25*), the RNA-binding domain of TTP is highly selective, optimally binding U-rich RNA sequences containing AUUUA or AUUUUA motifs (*25*−*27*).

Previously, we demonstrated that a 73 amino acid peptide containing the TTP tandem zinc finger domain, termed TTP73, formed high-affinity complexes with ARE substrates in a zinc-dependent manner (*26*, *28*). Several observations based on these and other studies also suggested that ARE recognition by this peptide may proceed via an "induced-fit" or "selected-fit" mechanism (*29*, *30*). First, heteronuclear single-quantum coherence (HSQC) analyses permitted resonance assignments for most residues within the N-terminal zinc finger in the absence of an RNA substrate, indicative of structural ordering within this motif (*28*). By contrast, virtually no residues within the C-terminal domain could be assigned, consistent with conformational heterogeneity in this region. Second, TTP73 association with cognate RNA targets induced large peak shifts in N-terminal zinc finger residues by HSQC and also permitted assignment of residues within the C-terminal finger (*28*). These data indicated that RNA binding was accompanied by dramatic changes in peptide conformation involving both zinc fingers. Third, independent structural analyses of the RNA-binding domain of a TTP family member, TIS11d, showed that both the N-terminal and C-terminal zinc fingers adopted similar folds when complexed with a nine-base recognition sequence (*31*). Finally, TTP73 binding to high-affinity RNA substrates is associated with a large negative change in heat capacity (*26*). This thermodynamic signature of hydrophobic surface area burial (*32*) without substantial changes in RNA structure (*26*) is consistent with NMR predictions of protein folding linked to RNA−peptide complex formation.

In this work, we have used tryptophan- (Trp-) substituted TTP73 analogues to evaluate localized conformational changes within each zinc finger motif in response to $Zn^{2+}$ coordination and RNA substrate binding, exploiting the sensitivity of Trp fluorescence to changes in its local environment (*33*). The design of Trp-substituted variants of the wild-type TTP73 peptide (TTP73 wt) was based on two principal criteria: (i) that the substituted Trp residues localize to regions likely to experience similar conformational changes in each zinc finger and (ii) that the Trp substitutions not interfere with the RNA-binding activity of the peptide. Trp substitutions at Phe11 and Phe49 were selected as the most promising conformational sensors, based on the following rationale. First, Phe11 and Phe49 occupy homologous positions in the N- and C-terminal zinc fingers of TTP, respectively, between the first two Cys residues comprising each $Cx_8Cx_5Cx_3H$ motif (Figure 1A). Second, Phe11 and Phe49 are conserved in the TTP family member TIS11d and are located in similar α-helical regions within each TIS11d zinc finger when bound to an ARE substrate (Figure 1B). Localization of these Phe residues within structured domains in the TIS11d−ARE complex indicated that modulation of peptide folding near these sites would likely influence the fluorescence properties of each Trp mutant, based on alterations in proximity to nonpolar surfaces and/or changes in solvent accessibility. In particular, Phe11 and Phe49 exhibit stacking potential with $Zn^{2+}$-coordinated His residues His27 and His65, respectively, in the TIS11d−ARE complex (Figure 1C,D). Furthermore, these Phe residues are maintained in close proximity (<3.5 Å) to the zinc ions and conserved $Zn^{2+}$-coordinated Cys residues (Cys17 and Cys55) of their respective zinc finger domains. Additional features indicated that Trp substitutions at Phe11 and Phe49 were unlikely to severely compromise the RNA-binding activity of the TTP tandem zinc finger peptides. Phe11 and Phe49 are not involved in coordination of $Zn^{2+}$, which is absolutely essential for RNA binding by TTP (*26*, *34*). Furthermore, these residues are distal to the RNA-binding interface in the TIS11d−ARE complex (Figure 1B).

On the basis of these considerations, TTP73 mutant peptides F11W and F49W were used to evaluate $Zn^{2+}$- and RNA-dependent conformational changes in the N- and C-terminal zinc finger domains of TTP, respectively. Alterations in local peptide structure were monitored by changes in the fluorescence quantum yields, emission peak wavelengths, and solvent accessibilities of Trp residues in each zinc finger. The relative stabilities of peptide structural transitions were compared using denaturant titration analyses. These studies indicate that the N- and C-terminal zinc finger domains exhibit very different structural responses to $Zn^{2+}$ binding in the absence of RNA. However, local peptide structures within both zinc finger domains exhibit extreme sensitivity to denaturant prior to RNA binding, consistent with conformational sampling between weakly folded states. Association with a cognate ARE substrate stabilized local peptide folding in both zinc fingers, based on resistance to chemical denaturation and dramatic decreases in both the quantum yields and solvent accessibilities of substituted tryptophan residues. By contrast, only the N-terminal zinc finger exhibited a similar structural response in the presence of ARE mutant substrates lacking either UUAU half-site. Considering these data together with previous NMR and thermodynamic analyses of interactions between the tandem zinc finger domain of TTP and RNA substrates, a model for ARE recognition involving conformational sampling and remodeling within the TTP zinc finger domains is discussed.

## EXPERIMENTAL PROCEDURES

*Materials*. The RNA substrates used in this study were denoted $ARE_9$ (5′-UUAUUUAUU-3′), $ARE_{13}$ (5′-AUUUAUUUAUUUA-3′), $ARE_{13}$-$AU_3U$ (5′-AUUUAUUUUUUUA-3′), $ARE_{13}$-$UU_3A$ (5′-AUUUUUUUAUUUA-3′), and $UC_{13}$ (5′-UCUCUCUCUCUCU-3′). Variants of RNA oligonucleotides containing 5′-linked fluorescein moieties are indicated by the prefix "Fl-". Each RNA substrate was synthesized, 2′-hydroxyl deprotected, and purified by Dharmacon Research (Lafayette, CO) or Integrated DNA Technologies (Coralville, IA). Lyophilized pellets were resuspended in 10 mM Tris-HCl (pH 8.0) and quantified by $A_{260}/A_{495}$ as previously described (*35*, *36*). Where required, 5′-hydroxyl RNA substrates were radiolabeled to specific activities of $(3-5) \times 10^3$ cpm/fmol using T4 polynucleotide kinase and [$\gamma$-$^{32}$P]ATP as described (*24*).

All synthetic peptides were synthesized, purified, and refolded by Albachem Ltd. (Edinburgh, Scotland) as described previously (*28*). TTP73 is a 73 amino acid peptide corresponding to the tandem zinc finger domain (residues 102−174) of human TTP (GenBank accession number

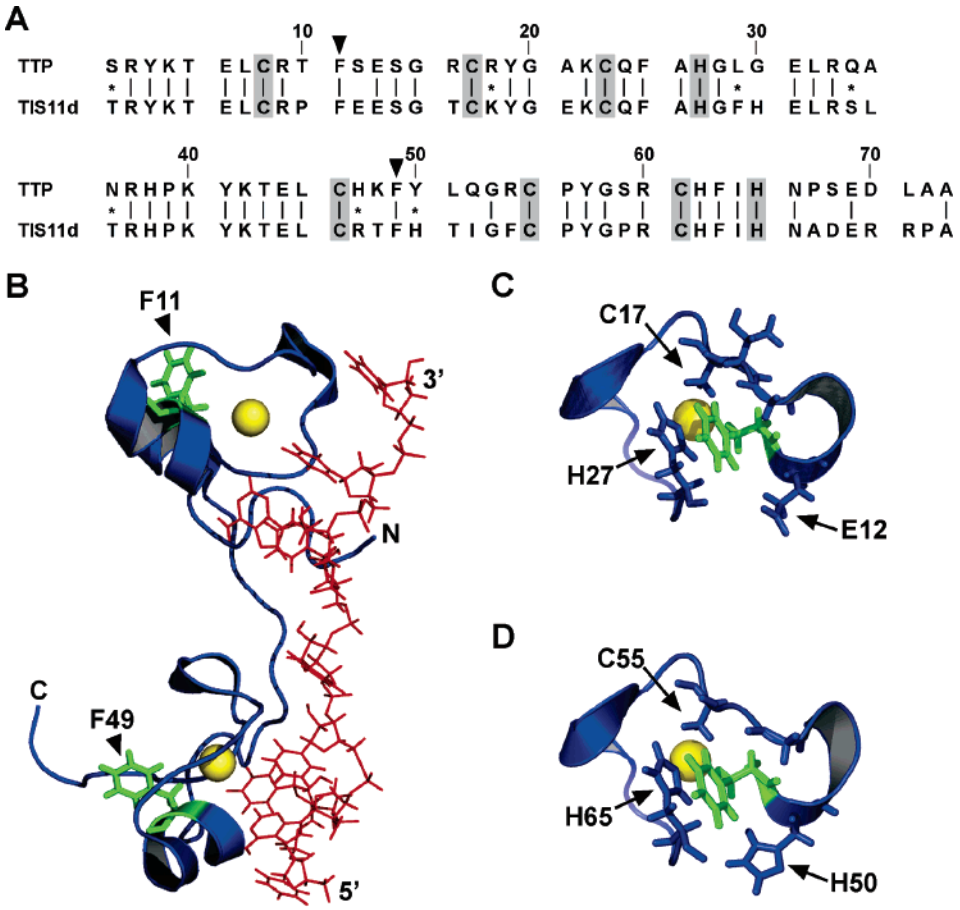


FIGURE 1: Selection of tryptophan substitution sites within the TTP tandem zinc finger domain. (A) Sequence alignment between the zinc finger domains of human TTP (GenBank accession number NP_003398; residues 102−174) and human TIS11d (GenBank accession number AAA91778; residues 152−224) was solved using the ALIGN program at the San Diego Supercomputer Center Biology Workbench (www.workbench.sdsc.edu). Lines indicate identical residues, while conservative substitutions are denoted by asterisks. $Zn^{2+}$-coordinating residues comprising each CCCH motif are shaded, and the positions of Phe residues mutated to Trp (F11 and F49) are indicated by arrowheads. (B) Structure of the TIS11d tandem zinc finger domain complexed with an ARE substrate (PDB number 1RGO from ref *31*) showing the location of residues corresponding to F11 and F49 of TTP73 in the folded peptide−RNA complex (green). The RNA substrate is in red, and zinc ions are indicated by yellow spheres. Enlarged views show the local environments of F11 (C) and F49 (D) (green) of TIS11d in the peptide−RNA complex.

NP_003398). Two additional peptides, termed TTP73 F11W and F49W, are TTP73 mutants containing individual Phe → Trp mutations at positions 11 and 49, respectively. Lyophilized peptides were resuspended in 10 mM Tris-HCl (pH 8.0) containing 2 mM dithiothreitol, frozen in aliquots at −80 °C, and quantified by Coomassie Blue-stained SDS−PAGE against a titration of BSA.

*RNA−Peptide Binding Studies.* Interactions between TTP73 peptides and RNA substrates were qualitatively evaluated using gel mobility shift assays (GMSAs). Binding reactions (10 $\mu$L total volume) containing varying concentrations of peptide and 0.2 nM $^{32}$P-labeled RNA substrate were assembled in RNA-binding buffer [10 mM Tris-HCl (pH 8.0) with 100 mM KCl, 2 mM dithiothreitol, 0.1 $\mu$g/$\mu$L bovine serum albumin, and 10% glycerol]. Heparin (0.2 $\mu$g/$\mu$L) was included to inhibit nonspecific interactions between peptides and RNA ligands. $ZnCl_2$ (5 $\mu$M) or EDTA (0.5 mM) was also added to the binding reactions where indicated. Prior to addition of RNA substrates, wild-type or mutant TTP73 peptides were incubated for 20 min at room temperature in binding mixtures to ensure coordination of $Zn^{2+}$. Previous experiments indicated that the RNA-binding activity of TTP73 was significantly impaired without this $Zn^{2+}$ preincubation step (data not shown). Following the addition of RNA, binding reactions were incubated on ice for 15 min and fractionated by electrophoresis through 6% (40:1 acrylamide:bisacrylamide) native gels at 4 °C. Gels were then dried and reaction products visualized by Phosphorimager scan (Amersham Biosciences, Piscataway, NJ).

Binding constants describing interactions between TTP73 peptides and fluorescein-conjugated RNA substrates were quantitatively measured using a fluorescence anisotropy-based assay, essentially as described (*26*). Fluorescence anisotropy was measured using a Beacon 2000 fluorescence polarization system (Panvera, Madison, WI) equipped with fluorescein excitation ($\lambda_{ex}$ = 490 nm) and emission ($\lambda_{em}$ = 535 nm) filters. In all experiments reported in this work, protein binding did not induce a change in the fluorescence quantum yield of Fl-RNA substrates. As such, the measured fluorescence anisotropy ($A_t$) of each binding reaction was interpreted as a function of the intrinsic anisotropy ($A_i$) and fractional concentration ($f_i$) of each fluorescent species using the equation (*37*, *38*):

$$A_t = \sum_i A_i f_i \quad (1)$$

Since the TTP73 peptide binds RNA substrates ≤13 nucleo-

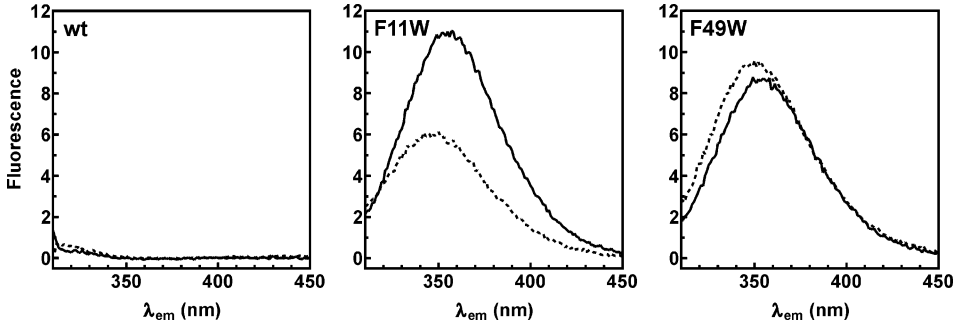


FIGURE 2: Fluorescence emission spectra of TTP73 peptides. Blank-corrected emission spectra ($\lambda_{ex}$ = 295 nm) of wild-type TTP73 (wt; left panel) and TTP73 mutant peptides F11W (center panel) and F49W (right panel) were measured following incubation for 20 min at room temperature in RNA-binding buffer containing EDTA (0.5 mM; solid line) or $ZnCl_2$ (25 $\mu$M; dotted line). Peptide concentrations were 2 $\mu$M for each sample. Spectral normalization was omitted to permit comparison of relative fluorescence quantum yields between peptides.

tides in length via 1:1 stoichiometry (*26*), measurement of $A_t$ across samples containing varying concentrations of peptide where RNA concentration is limiting (i.e., $[TTP73]_{free} \approx [TTP73]_{total}$) thus permits resolution of binding constants by the equation:

$$A_t = \frac{A_R + A_{PR}K[TTP73]}{1 + K[TTP73]} \quad (2)$$

Here, $A_R$ and $A_{PR}$ represent the intrinsic anisotropy values of the free and protein-associated Fl-RNA substrates, respectively, while $K$ represents the equilibrium association constant. $A_R$ was measured directly from binding reactions lacking peptide ($n \geq 3$), while all other constants were solved by nonlinear least-squares regression of $A_t$ versus [TTP73] plots using PRISM v3.0 (GraphPad, San Diego, CA).

*Tryptophan Fluorescence and Quenching Analyses.* Tryptophan fluorescence was measured using a Cary Eclipse spectrofluorometer (Varian Instruments, Walnut Creek, CA) fitted with a submicrocell. Samples (60 $\mu$L total volume) containing peptide (2−2.5 $\mu$M) were prepared with $ZnCl_2$ (25 $\mu$M) or EDTA (0.5 mM) as described for fluorescence anisotropy analyses (above). Heparin was omitted from reactions employed for tryptophan fluorescence assays, since protein contaminants in commercially available heparin preparations were found to contribute significant background fluorescence (data not shown). RNA substrates were added at equimolar concentrations where indicated, and tryptophan emission spectra were measured using 295 nm excitation with 10 nm bandwidth for both excitation and emission monochromators. For measurements of solvent accessibility, varying concentrations of potassium iodide or acrylamide were added after 30 min of RNA−peptide complex formation. Stern−Volmer quench constants ($K_{SV}$) were extracted from measured emission at 350 nm ($F$) as a function of quencher concentration ([Q]) using the equation:

$$F_0/F = 1 + K_{SV}[Q] \quad (3)$$

where $F_0$ represents the fluorescence intensity in the absence of the quencher (*33*). For denaturant titration experiments, varying concentrations of GnHCl were added after 30 min of RNA−peptide complex formation and then incubated for a further 30 min at room temperature prior to measurement of tryptophan emission spectra.

Table 1: Emission Properties of TTP73 Phe → Trp Mutant Peptides

| peptide | $Zn^{2+}$ | RNA | emission peak (nm)[a] | relative intensity at 350 nm[a,b] |
|---|---|---|---|---|
| F11W | − | − | 356 ± 1 | 1.0 |
| | + | − | 346 ± 1 | 0.51 ± 0.06 |
| | + | $UC_{13}$ | 347 ± 2 | 0.54 ± 0.02 |
| | + | $ARE_{13}$ | 347 ± 1 | 0.30 ± 0.04 |
| | + | $ARE_{13}$-$AU_3U$ | 348 ± 1 | 0.30 ± 0.03 |
| | + | $ARE_{13}$-$UU_3A$ | 347 ± 2 | 0.33 ± 0.05 |
| F49W | − | − | 354 ± 1 | 1.0 |
| | + | − | 352 ± 1 | 1.11 ± 0.06 |
| | + | $UC_{13}$ | 352 ± 1 | 0.98 ± 0.04 |
| | + | $ARE_{13}$ | 354 ± 1 | 0.68 ± 0.06 |
| | + | $ARE_{13}$-$AU_3U$ | 352 ± 2 | 1.01 ± 0.05 |
| | + | $ARE_{13}$-$UU_3A$ | 352 ± 1 | 0.99 ± 0.05 |

[a] Mean ± $\sigma_{n-1}$ for $n \geq$ three independent experiments. [b] Intensity relative to $-Zn^{2+}$ for each peptide.

## RESULTS

*The Zinc Fingers of TTP Exhibit Different Structural Responses upon Coordination of $Zn^{2+}$.* $Zn^{2+}$-dependent changes in the conformation of the TTP zinc finger domains were initially assessed by measuring Trp emission spectra of the TTP73 F11W and F49W peptides in the presence and absence of zinc (Figure 2). Fluorescence emission from the wild-type TTP73 peptide was barely detectable above background. Since TTP73 wt lacks Trp residues, this confirmed that other aromatic residues (Phe and Tyr) do not significantly contribute to total fluorescence emission from the TTP73 mutant peptides measured under these conditions. The intensity of fluorescence emission from TTP73 F11W was decreased by 50% in the presence of $Zn^{2+}$, indicating that the conformation of the N-terminal zinc finger was sensitive to the presence of the cation. The F11W fluorescence emission peak was also blue shifted from 356 to 346 nm (Table 1), consistent with transition of the Trp residue side chain to a less polar environment in a $Zn^{2+}$-dependent manner (*33*). By contrast, neither the fluorescence quantum yield nor emission peak wavelength of the F49W mutant was significantly modified by $Zn^{2+}$, indicating that the C-terminal zinc finger does not experience the same conformational transition as the N-terminal finger in the presence of the cation.

As an independent measure of $Zn^{2+}$-dependent conformational changes in the TTP zinc finger domains, the solvent accessibilities of Trp residues at positions 11 and 49 were analyzed by collisional quenching in the presence or absence

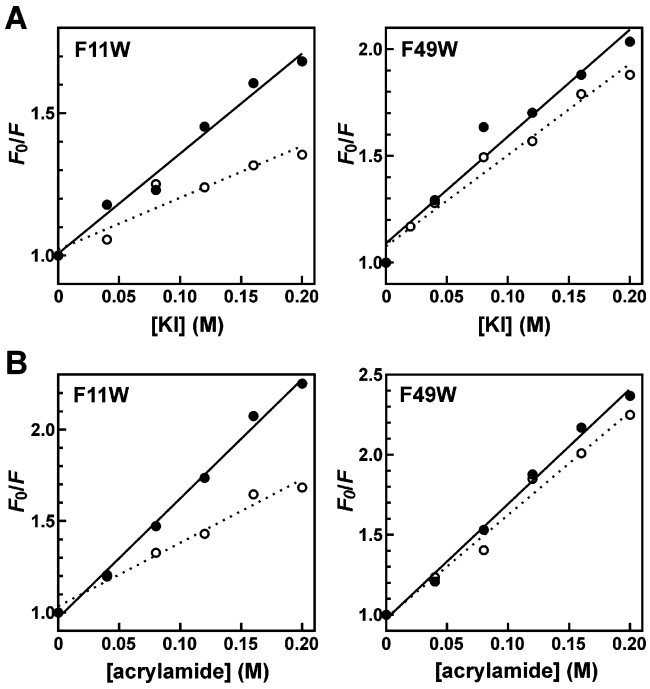


FIGURE 3: Effects of $Zn^{2+}$ coordination on solvent accessibility of Trp residues at TTP73 positions 11 and 49. Stern−Volmer plots were prepared from fluorescence emission ($\lambda_{ex}$ = 295 nm; $\lambda_{em}$ = 350 nm) of TTP73 F11W or F49W peptide samples (2.5 $\mu$M each) containing varying concentrations of potassium iodide (A) or acrylamide (B) as described under Experimental Procedures. Prior to assembly of quenching reactions, TTP73 mutant peptides were incubated with EDTA (solid circles, solid line) or $ZnCl_2$ (open circles, dotted line) as in Figure 2.

Table 2: Stern−Volmer Quench Constants for TTP73 Phe → Trp Mutant Peptides

| peptide | $Zn^{2+}$ | RNA | quencher | $K_{SV}$ ($M^{-1}$)[a] | *n* |
|---|---|---|---|---|---|
| F11W | − | − | KI | 3.4 ± 0.2 | 3 |
| | + | − | KI | 1.5 ± 0.2 | 3 |
| | − | − | acrylamide | 6.0 ± 0.5 | 3 |
| | + | − | acrylamide | 3.6 ± 0.3 | 3 |
| | + | $UC_{13}$ | acrylamide | 4.4 ± 0.2 | 3 |
| | + | $ARE_{13}$ | acrylamide | 1.4 ± 0.3 | 3 |
| | + | $ARE_{13}$-$AU_3U$ | acrylamide | 1.5 ± 0.4 | 2 |
| | + | $ARE_{13}$-$UU_3A$ | acrylamide | 1.5 ± 0.3 | 2 |
| F49W | − | − | KI | 4.7 ± 0.3 | 3 |
| | + | − | KI | 4.2 ± 0.1 | 4 |
| | − | − | acrylamide | 6.4 ± 0.4 | 4 |
| | + | − | acrylamide | 6.4 ± 0.6 | 4 |
| | + | $UC_{13}$ | acrylamide | 7.3 ± 0.6 | 3 |
| | + | $ARE_{13}$ | acrylamide | 1.3 ± 0.2 | 3 |
| | + | $ARE_{13}$-$AU_3U$ | acrylamide | 5.9 ± 0.2 | 2 |
| | + | $ARE_{13}$-$UU_3A$ | acrylamide | 5.6 ± 0.4 | 3 |

[a] Mean ± $\sigma_{n-1}$ for *n* independent experiments where $n > 2$ or mean ± spread for $n = 2$.

of $Zn^{2+}$. For the TTP73 F11W peptide, $Zn^{2+}$ decreased Stern−Volmer constants ($K_{SV}$) derived from titrations of iodide or acrylamide quenchers by 56% and 40%, respectively (Figure 3 and Table 2), indicating significant loss of solvent accessibility concomitant with $Zn^{2+}$-dependent conformational changes in the N-terminal finger. Conversely, $Zn^{2+}$ induced no significant changes in $K_{SV}$ values for the TTP73 F49W peptide, supporting the model of little or no net $Zn^{2+}$-dependent alterations of peptide conformation in this region of the C-terminal zinc finger domain. Control experiments with free tryptophan confirmed that the $Zn^{2+}$ concentrations employed in this study did not systematically influence the fluorescence quantum yield or solvent accessibility of this amino acid (data not shown). For both TTP73 mutant peptides, fluorescence emission from Trp residues was more efficiently quenched by acrylamide versus iodide (Table 2). This observation is consistent with previous studies showing that acrylamide quenches the fluorescence of a tryptophan analogue by electron transfer whereas iodide quenching relies on a collisional heavy atom effect (*39*). As a result, acrylamide can quench fluorescent compounds from greater distances in solution, rendering it a more effective quenching agent.

*TTP73 F11W and F49W Form High-Affinity Complexes with ARE Substrates*. Previously, we demonstrated that the TTP73 wt peptide forms high-affinity ($K_d$ < 20 nM) interactions with RNA substrates of the form $UUAU_nAUU$, where *n* ranges from 2 to 5 (*26*). To ensure that the Trp substitutions at positions 11 and 49 of TTP73 did not dramatically modify its RNA-binding activity, we employed gel mobility shift assays (GMSAs) and fluorescence anisotropy-based methods to characterize interactions between RNA substrates and the TTP73 F11W or F49W mutants. By GMSA, both the TTP73 F11W and F49W peptides formed single, comigrating RNA−peptide complexes with either 9-base ($ARE_9$; Figure 4A) or 13-base ($ARE_{13}$; data not shown) RNA substrates containing canonical TTP binding motifs. Sequence specificity for ARE ligands did not appear to be compromised, since no peptide binding was detected to an irrelevant 13-base RNA substrate ($UC_{13}$; Figure 4A), even at peptide concentrations up to 2.5 $\mu$M (data not shown). Quantitative analyses using fluorescence anisotropy (Figure 4B) indicated that association of TTP73 F11W and F49W peptides with fluorescein-labeled ARE substrates was well resolved by a binary equilibrium binding model (eq 2). Derived bimolecular association constants showed a small but not statistically significant decrease in the affinity of TTP73 F11W for each of the 9- and 13-base ARE substrates relative to the wild-type peptide (Table 3). Binding of the F49W mutant to each ARE ligand returned slightly weaker dissociation constants than for the F11W peptide ($K_d$ = 6.8−8.3 nM); however, binding affinities yielding $K_d$ values of up to 20 nM have been observed between TTP73 wt and other ARE substrates exhibiting potent mRNA-destabilizing activity (*10*, *28*). This demonstration of specific, high-affinity interactions between each TTP73 Phe → Trp mutant and ARE substrates validated the use of these peptides as probes of local protein structure in peptide−ARE complexes.

*Cognate ARE Binding Induces Conformational Changes within Both Zinc Fingers of TTP*. Following the demonstration that the TTP73 F11W and F49W peptides were competent for high-affinity ARE binding, fluorescence emission and collisional quenching studies were performed to identify RNA substrate-dependent changes in the conformations of each TTP zinc finger domain. RNA and peptide components were assembled at concentrations at least 300-fold above $K_d$ (2.5 $\mu$M of each reagent) to promote quantitative formation of RNA−peptide complexes. Fluorescence emission from both the F11W and F49W mutants was decreased by approximately 40% upon binding the $ARE_{13}$ substrate relative to reactions supplemented with $Zn^{2+}$ alone (Figure 5A and Table 1). RNA-dependent changes in the fluorescence of each peptide were specific for the high-

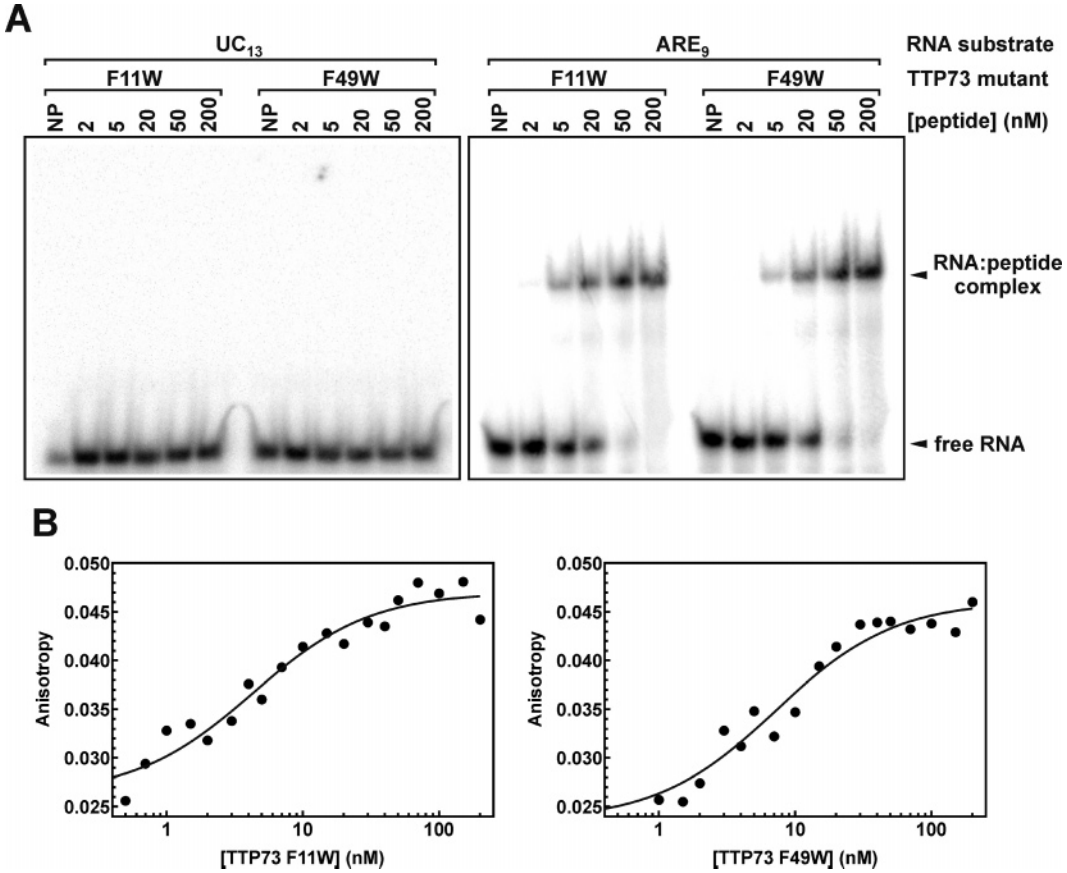


FIGURE 4: Association of TTP73 mutant peptides with RNA substrates. (A) Binding reactions containing $^{32}$P-labeled RNA substrates (0.2 nM) and varying concentrations of TTP73 F11W or F49W peptides were fractionated by native gel electrophoresis. The position of the complex formed by peptide binding to the $ARE_9$ substrate is indicated. (B) Fluorescence anisotropy ($\lambda_{ex}$ = 490 nm; $\lambda_{em}$ = 535 nm) was measured for binding reactions containing the Fl-$ARE_9$ RNA substrate (0.2 nM) and titrations of TTP73 F11W (left panel) or F49W (right panel) peptides assembled as described under Experimental Procedures. Association constants describing the interaction of each peptide with the Fl-$ARE_9$ ligand were resolved by nonlinear regression using eq 2 (solid lines).

Table 3: Equilibrium Binding of TTP73 Phe → Trp Mutant Peptides to RNA Substrates

| RNA | peptide | $K$ ($\times 10^8$ M$^{-1}$)[a] | $K_d$ (nM)[b] | $n$ |
|---|---|---|---|---|
| Fl-$ARE_9$ | wt | 3.3 ± 0.4[c] | 3.0 | 3 |
| | F11W | 2.23 ± 0.05 | 4.5 | 2 |
| | F49W | 1.46 ± 0.07 | 6.8 | 2 |
| Fl-$ARE_{13}$ | wt | 2.8 ± 0.5[c] | 3.6 | 4 |
| | F11W | 1.7 ± 0.2 | 5.9 | 2 |
| | F49W | 1.2 ± 0.1 | 8.3 | 2 |

[a] Mean ± $\sigma_{n-1}$ for $n$ independent experiments where $n > 2$ or mean ± spread for $n = 2$. [b] $K_d$ estimated as $1/K$. [c] Wild-type TTP73 binding data are from ref *26*.

affinity ARE ligand, since substitution of a nonspecific RNA substrate ($UC_{13}$) did not significantly influence the fluorescence properties of either mutant relative to reactions lacking RNA. This demonstrates that the diminished fluorescence emission from the F11W and F49W mutants is a consequence of ARE substrate binding and not a trivial result of collisional quenching by RNA in solution. Trp residues in both the 11 and 49 positions of TTP73 also displayed dramatic decreases in solvent accessibility when bound to an ARE ligand (Figure 5B). $ARE_{13}$ substrate binding decreased Stern−Volmer constants derived from acrylamide titrations by 60% for the F11W peptide and 80% for the F49W mutant (Table 2). Like the RNA-dependent changes in fluorescence emission, restriction of solvent accessibility within each zinc finger domain was specific for ARE binding, since acrylamide quenching efficiency was not significantly modulated by the presence of the $UC_{13}$ substrate for either TTP73 mutant peptide. Taken together, the decreased fluorescence emission and restricted solvent accessibility of Trp residues in both the TTP73 F11W and F49W peptides in response to ARE binding indicate that both zinc finger domains are structurally modified by association with cognate ARE substrates.

Additional experiments investigated the conformational events resulting from TTP73 peptide association with suboptimal RNA substrates. For ARE ligands lacking adenosine residues defining either the 5′- ($ARE_{13}$-$UU_3A$) or 3′- ($ARE_{13}$-$AU_3U$) UUAU half-sites, wild-type TTP73 exhibits impaired but still significant binding activity ($K_d \approx$ 55 nM) (*26*). TTP73 F11W exhibited significant decreases in both Trp fluorescence emission and solvent accessibility upon binding to either of these ARE half-site mutant ligands, suggesting structural consequences similar to those observed with the cognate ARE substrate (Tables 1 and 2). However, the fluorescence characteristics of the TTP73 F49W peptide were not significantly influenced by association with either ARE half-site mutant. These data indicate that conformational adaptation of the N-terminal finger can occur independently of the C-terminal finger and that RNA-dependent folding of the C-terminal finger may structurally discriminate TTP73−RNA complexes containing cognate versus near-cognate ARE substrates.

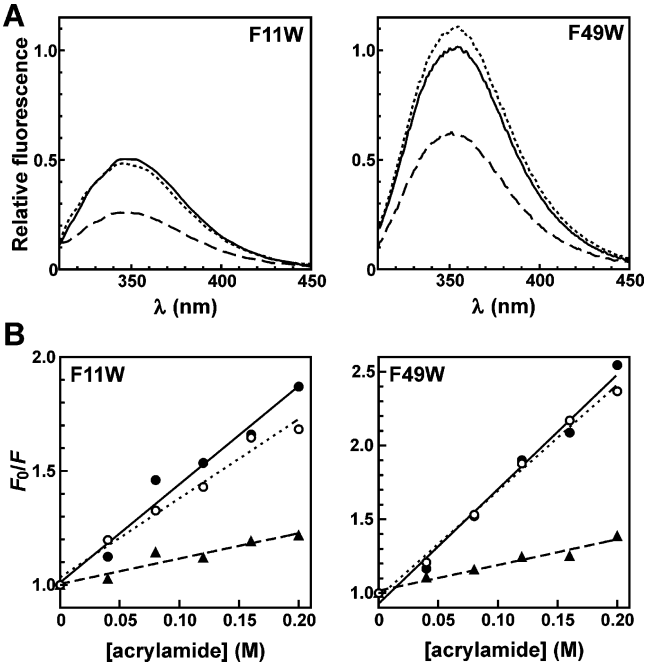


FIGURE 5: RNA-dependent changes in fluorescence emission and solvent accessibility of Trp residues at TTP73 positions 11 and 49. (A) Blank-corrected emission spectra ($\lambda_{ex}$ = 295 nm) of TTP73 F11W (2.5 $\mu$M; left panel) or F49W (2.5 $\mu$M; right panel) preincubated with $ZnCl_2$ (25 $\mu$M) in the absence (dotted line) or presence of RNA substrates (2.5 $\mu$M) $UC_{13}$ (solid line) or $ARE_{13}$ (dashed line). Fluorescence spectra from each sample are shown relative to the emission of reactions containing EDTA (Figure 2). (B) Acrylamide quenching of $Zn^{2+}$-conjugated TTP73 F11W (left panel) or F49W (right panel) in the absence (open circles, dotted line) or presence of RNA substrates $UC_{13}$ (solid circles, solid line) or $ARE_{13}$ (triangles, dashed line) resolved by Stern−Volmer plot. The sensitivity of TTP73−ARE equilibria to ionic strength precluded the use of potassium iodide as a collisional quencher in these experiments (*26*).

*ARE Binding Stabilizes Folded States Involving Both Zinc Fingers of TTP*. The preceding experiments indicated that at least one structural transition is experienced by Trp in position 49 of TTP73 in response to binding a cognate ARE ligand. By contrast, at least two distinct folding events were observed for Trp in position 11: one dependent on $Zn^{2+}$ and another on binding to an ARE substrate. In order to evaluate the relative stabilities of each conformational transition, the fluorescence properties of TTP73 F11W and F49W peptides were monitored in the presence and absence of RNA substrates across titrations of the chemical denaturant, guanidine hydrochloride (GnHCl).

In the presence of $Zn^{2+}$ but the absence of RNA, the TTP73 F49W peptide displayed enhanced fluorescence emission with increasing concentrations of GnHCl (Figure 6A). Emission from the F49W mutant increased by approximately 70% at 100 mM GnHCl (Figure 6B) but was not significantly elevated beyond this intensity, even at GnHCl concentrations as high as 3 M (data not shown). The increase in fluorescence of F49W as a function of denaturant concentration is consistent with structural relaxation near the Trp residue in the C-terminal zinc finger. Curiously, this transition was extremely sensitive to GnHCl, with the half-maximal effect observed at only 1−2 mM denaturant. However, the lack of approach to a lower asymptote at minimal denaturant concentrations precluded quantitative resolution of domain unfolding free energies by linear extrapolation (*40*, *41*).

Similar GnHCl denaturation experiments performed with TTP73 F49W in the presence of the $UC_{13}$ RNA substrate closely mirrored the unfolding transition of TTP73 F49W in the absence of RNA. However, association of the F49W peptide with the $ARE_{13}$ substrate significantly stabilized a peptide conformation in the C-terminal finger, with half-maximal unfolding observed at approximately 100 mM GnHCl (Figure 6B). The amplitude of the fluorescence change in the presence of the $ARE_{13}$ ligand is enhanced relative to the other data sets because the fluorescence intensity of the TTP73 F49W−$ARE_{13}$ complex in the absence of GnHCl ($F_0$) is lower than those of the F49W peptide alone or in the presence of the $UC_{13}$ substrate (Table 1). The extreme sensitivity of TTP73 F49W fluorescence to GnHCl suggests that the C-terminal zinc finger is very weakly folded or presents a dynamic population of conformations near position 49 in the absence of an ARE. The significant decrease in denaturant sensitivity exhibited in the presence of the $ARE_{13}$ substrate may thus represent stabilization of one or a small subset of peptide conformations within the C-terminal zinc finger by association with a cognate RNA ligand.

Like the F49W mutant, TTP F11W displayed enhanced fluorescence emission with increasing concentrations of GnHCl in the presence of $Zn^{2+}$ but absence of RNA (Figure 7A). Unlike F49W, however, monitoring fluorescence intensity at 350 nm as a function of denaturant concentration revealed two distinct conformational transitions for the F11W peptide. The weakest transition enhanced fluorescence intensity by approximately 30% (Figure 7B inset, open circles; cf. 0 M GnHCl versus 0.01 M), with half-maximal change observed at 1 mM GnHCl. The second transition was more gradual, with fluorescence emission increasing by approximately 100% across a broad range of GnHCl concentrations above 0.6 M. In addition to increases in fluorescence emission, high concentrations of GnHCl also reversed the blue-shifted position of the F11W peak induced by $Zn^{2+}$ coordination (Figure 7A). Evaluation of F11W emission spectra across the GnHCl titration showed that loss of the blue-shifted emission peak accompanied the second (i.e., more stable) transition and was most pronounced between 0.6 and 2 M GnHCl (Figure 7C). The concurrent increase in fluorescence intensity and loss of the emission peak blue shift of TTP73 F11W observed at GnHCl concentrations above 0.6 M indicate that this more stable conformational transition likely involves the release of $Zn^{2+}$. By contrast, the weaker transition may represent conformational heterogeneity near position 11 of TTP73, similar to the model proposed for F49W (above). However, the amplitude of the fluorescence change accompanying this weaker folding transition is smaller for F11W than for F49W, suggesting that the distribution or flexibility of local peptide conformations may be more constrained in the N-terminal finger relative to the C-terminal domain.

Similar to the F49W example, inclusion of the nonbinding $UC_{13}$ RNA substrate did not significantly influence the sensitivity of TTP73 F11W fluorescence to GnHCl (Figure 7B, closed circles). Addition of the $ARE_{13}$ substrate, however, dramatically stabilized the weaker transition, delaying

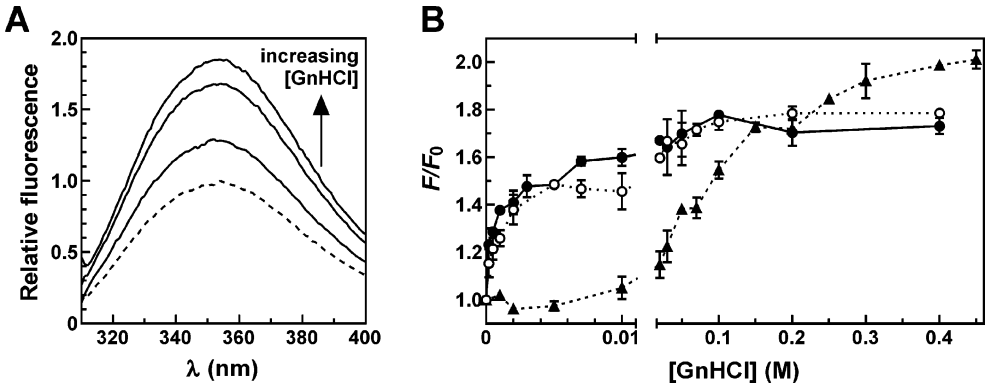


FIGURE 6: Denaturation of TTP73 F49W by GnHCl titration. (A) TTP73 F49W (2.5 $\mu$M) samples preincubated with $ZnCl_2$ (25 $\mu$M) were treated with 0.5, 10, or 100 mM GnHCl for 30 min at room temperature before measurement of fluorescence emission spectra ($\lambda_{ex}$ = 295 nm). Blank-corrected spectra are shown normalized to the sample lacking GnHCl (dashed line). (B) Fluorescence emission ($\lambda_{ex}$ = 295 nm; $\lambda_{em}$ = 350 nm) of TTP73 F49W across a titration of GnHCl in the absence (open circles, dotted line) or presence of equimolar concentrations of RNA substrates $UC_{13}$ (solid circles, solid line) or $ARE_{13}$ (triangles, dashed line). Fluorescence measurements were normalized to the emission of each F49W−RNA combination lacking GnHCl ($F_0$). Points represent the mean ± spread of duplicate independent experiments.

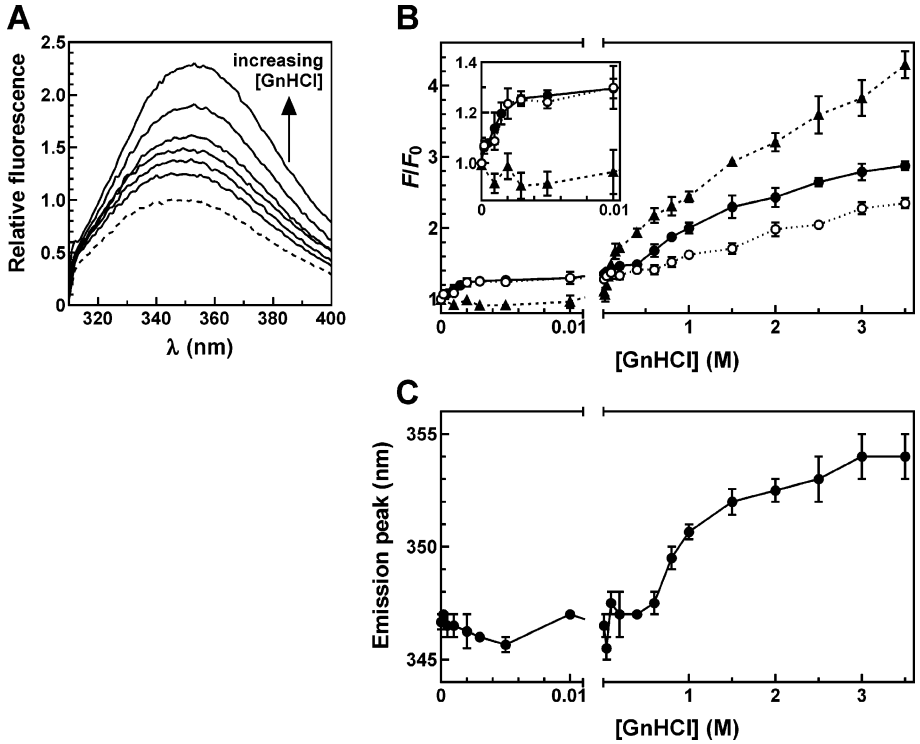


FIGURE 7: Denaturation of TTP73 F11W by GnHCl titration. (A) TTP73 F11W (2.5 $\mu$M) samples preincubated with $ZnCl_2$ (25 $\mu$M) were treated with 0.005, 0.02, 0.1, 1, 2, or 3 M GnHCl for 30 min at room temperature before measurement of fluorescence emission spectra ($\lambda_{ex}$ = 295 nm). Blank-corrected spectra are shown normalized to the sample lacking GnHCl (dashed line). (B) Fluorescence emission ($\lambda_{ex}$ = 295 nm; $\lambda_{em}$ = 350 nm) of TTP73 F11W across a titration of GnHCl in the absence (open circles, dotted line) or presence of equimolar concentrations of RNA substrates $UC_{13}$ (solid circles, solid line) or $ARE_{13}$ (triangles, dashed line), normalized to emission from each F11W−RNA combination lacking GnHCl ($F_0$). Points represent the mean ± $\sigma_{n-1}$ of triplicate independent experiments. (C) Positions of emission intensity peaks were extracted from emission spectra and plotted for TTP73 F11W samples across a titration of GnHCl in the absence of RNA. Each point represents the mean ± $\sigma_{n-1}$ of triplicate independent experiments.

denaturant-induced increases in fluorescence intensity to GnHCl concentrations >100 mM (Figure 7B, triangles). Also similar to F49W, the change in fluorescence accompanying the initial F11W unfolding event in the presence of the ARE ligand exhibited a greater amplitude than reactions lacking this substrate, owing to the decreased fluorescence of the F11W−$ARE_{13}$ complex in the absence of GnHCl ($F_0$; Table 1). The addition of RNA substrates did not appear to significantly influence the more stable conformational transition of F11W, based on similarities in the amplitude of fluorescence change, the GnHCl concentration dependence of this transition (Figure 7B), or loss of the emission peak blue shift (data not shown). Together, these data support a model whereby the conformation of the N-terminal zinc finger of TTP is substantially more ordered by the coordination of $Zn^{2+}$ than the C-terminal finger. Second, the GnHCl titration experiments indicate that, even in the presence of $Zn^{2+}$, local peptide structures within both the N- and C-terminal zinc finger domains of TTP retain some degree of flexibility or structural heterogeneity but are further constrained and/or stabilized concomitant with high-affinity RNA ligand binding.

## DISCUSSION

To date, no high-resolution molecular structure has been reported for the tandem zinc finger domain of TTP or any related CCCH zinc finger peptide in the absence of RNA. In this study, we provide evidence for distinct structural consequences within each zinc finger of TTP in response to association of zinc ions or RNA substrates. Furthermore, the RNA sequence dependence of folding events within C-terminal zinc finger likely contributes to discrimination of cognate versus near-cognate RNA ligands.

*$Zn^{2+}$-Dependent Changes in Conformation of the TTP Zinc Finger Domains*. $Zn^{2+}$-dependent folding of the N-terminal zinc finger was revealed by decreased quantum yield of TTP73 F11W, significantly blue-shifted emission from this peptide, and decreased solvent accessibility of the Trp residue at position 11 in the presence of zinc (Tables 1 and 2). Denaturant titration experiments also demonstrated considerable folded stability for the $Zn^{2+}$-associated N-terminal zinc finger. Half-maximal reversal of the $Zn^{2+}$-induced F11W emission peak blue shift ($[GnHCl]_{1/2}$) was observed at approximately 0.8 M GnHCl, concomitant with increases in fluorescence intensity. By comparison, the structures of some well-characterized globular proteins show similar sensitivities to this denaturant, including α-lactalbumin ($[GnHCl]_{1/2}$ = 1.1 M) (*42*) and maltose binding protein ($[GnHCl]_{1/2}$ = 1.0 M) (*43*). Together, these data indicate that the N-terminal zinc finger of TTP73 adopts a stable conformation following $Zn^{2+}$ coordination that includes partial burial of the residue at position 11. A previous study also suggested a defined $Zn^{2+}$-dependent conformation for the N-terminal zinc finger of the TTP-related protein TIS11d, since HSQC spectra could not be resolved in the absence of $Zn^{2+}$ but were well dispersed in the presence of the cation (*31*). Also, HSQC analyses permitted resolution of most residues in the N-terminal zinc finger of human (*28*) and murine (*44*) TTP in the presence of $Zn^{2+}$ but the absence of RNA.

While efficient and stable coordination of $Zn^{2+}$ to the N-terminal zinc finger domain was anticipated from the literature and corroborated by this study, no data describing $Zn^{2+}$-dependent conformational changes in the TTP C-terminal zinc finger have been reported. Although residues within the C-terminal zinc finger domain of TIS11d were resolved by HSQC in the presence of $Zn^{2+}$ and absence of RNA (*31*), this was not the case for the wild-type TTP73 peptide under these conditions (*28*). In the current study, the Trp residue inserted at position 49 of TTP73 revealed no significant changes in quantum yield, emission peak wavelength, or solvent accessibility in the presence of $Zn^{2+}$ (Tables 1 and 2). On the basis of the TIS11d−ARE structure (*31*), Trp residues in positions 11 and 49 of TTP73 were anticipated to exist in similarly folded environments (Figure 1C,D), particularly with respect to potential stacking interactions between each Trp and $Zn^{2+}$-coordinated His residues (His27 and His65). While this or a similar conformation is possible for the N-terminal zinc finger domain in the presence of $Zn^{2+}$ alone (above), we conclude that such an arrangement for the TTP73 C-terminal finger is highly improbable in the absence of RNA given the insensitivity of TTP73 F49W fluorescence to $Zn^{2+}$. High-affinity binding between TTP73 F49W and ARE substrates (Table 3) refutes the possibility that the F49W mutation substantially impairs or precludes $Zn^{2+}$ coordination to the C-terminal zinc finger, since (i) association of TTP73 with ARE substrates is absolutely dependent on $Zn^{2+}$ (*26*), (ii) mutation of $Zn^{2+}$-coordinating residues in the C-terminal zinc finger domain abrogate RNA-binding activity (*34*), and (iii) RNA binding by the N-terminal finger alone exhibits only micromolar affinity (*45*). An alternate possibility is that $Zn^{2+}$ binds but might not tightly coordinate with the C-terminal zinc finger in the absence of an RNA substrate. This would account for the independence of TTP73 F49W fluorescence with respect to $Zn^{2+}$, the extreme sensitivity of F49W fluorescence to GnHCl in the absence of RNA, and the lack of resolvable HSQC assignments in this domain (*28*). Furthermore, $Co^{2+}$ titrations performed by Worthington et al. suggest substoichiometric interaction of metal ions with the C-terminal zinc finger of TTP (*46*). While 1:1 binding was observed between $Co^{2+}$ and the N-terminal zinc finger of TTP, comparable experiments with the tandem zinc finger domain yielded an average binding ratio of 1.7 mol of metal ion/mol of peptide. Taken together, these data suggest that the conformation of the C-terminal finger might sample from a population of structures, possibly involving dynamic association of $Zn^{2+}$, which may be coupled to the specificity of RNA substrate recognition (discussed below).

*RNA-Dependent Changes in Conformation of the TTP Zinc Finger Domains*. Previous NMR and thermodynamic studies indicated that association with a cognate RNA substrate was accompanied by conformational changes within both zinc finger domains of TTP or TIS11d and defined a cognate substrate as an RNA ligand containing tandem UUAU motifs (*26*, *28*, *31*). From the current study, this model is supported by significant decreases in fluorescence emission from both TTP73 F11W and F49W when bound to the cognate $ARE_{13}$ substrate (Table 1). Furthermore, the F11W and F49W peptides exhibited virtually equivalent Stern−Volmer quench constants upon binding the $ARE_{13}$ ligand (Table 2), consistent with placement of each Trp residue in a similar structural environment. Localization of the Trp substitutions distal to the RNA-binding interface of each zinc finger indicates that the ARE-dependent changes in Trp fluorescence likely result from conformational changes in the peptide rather than steric effects from the associated RNA ligand. However, two observations illustrate subtle differences in folding between the TTP zinc finger domains, even when bound to RNA. First, emission from the F49W peptide was not blue shifted by ARE-induced peptide folding, suggesting a more polar environment for the substituted Trp in the C-terminal versus N-terminal zinc fingers (Table 1). Second, the F49W peptide retained an increased fluorescence quantum yield relative to F11W in the presence of the ARE (Table 1). Differences in local environments could be due to the residues flanking the proposed Trp−His stack in each zinc finger (Figure 1). On the basis of the TIS11d−ARE structure, the Trp in position 11 would be positioned within 3.4 Å of Glu12 (Ser in TTP) in the peptide−ARE complex, while the Trp in position 49 would be juxtaposed by His50 (3.2 Å; Tyr in TTP). The adjacent residues could alter the orientation or flexibility of Trp residue side chains in the folded zinc finger domains or could differentially quench Trp emission (*47*).

While both zinc finger domains exhibited conformational changes upon binding to a cognate RNA ligand, only the N-terminal finger displayed similar folding behavior when

associated with near-cognate ARE substrates, in which either the 5′- or 3′-UUAU motif was mutated (Tables 1 and 2). One possibility is that the "$Zn^{2+}$-primed" N-terminal finger binds the RNA ligand first and, hence, occupies the first accessible UUAU half-site. Recognition of a cognate site would then be achieved by comparable structural rearrangements within the C-terminal finger, requiring a second UUAU motif immediately upstream of the first. In this manner, the conformational status of the C-terminal finger may constitute the final step in discrimination of RNA ligands. While U-rich RNA sequences containing a single UAUU motif can bind the TTP tandem zinc finger domain, these ligands bind 10−20-fold more weakly than a cognate RNA-binding site (*26*) and are incapable of directing rapid cytoplasmic mRNA decay through TTP (*10*).

*Might RNA Substrate Recognition Involve Conformational Sampling within TTP Zinc Finger Domains?* The fluorescence of Trp residues in both positions 11 and 49 of TTP73 exhibited extreme sensitivity to GnHCl in the absence of an ARE ligand (Figures 6 and 7). These data could denote either thermodynamically weak local peptide conformations and/or dynamic populations of heterogeneously folded structures within each zinc finger. With respect to the N-terminal zinc finger, some support for the latter possibility comes from previous NMR studies where superimposing refined structures of the $Zn^{2+}$-coordinated N-terminal zinc finger of murine TTP revealed significant structural heterogeneity in the absence of RNA (*44*). The distribution of local peptide conformations was particularly diverse among amino acid side chains not involved in coordination of $Zn^{2+}$. For the C-terminal zinc finger domain, the lack of defined HSQC peaks in the absence of an RNA substrate (*28*) coupled with insensitivity of TTP73 F49W fluorescence to $Zn^{2+}$ (this study) also supports a model of heterogeneous peptide conformations prior to ARE binding. However, several observations suggest that association of the TTP RNA-binding domain with cognate RNA substrates is coupled to restriction of conformational heterogeneity within each zinc finger domain. First, emission from Trp residues in positions 11 and 49 of TTP73 became significantly less sensitive to GnHCl upon binding to an ARE ligand (Figures 6B and 7C), consistent with RNA-dependent contributions to the thermodynamic stability of peptide folding within each zinc finger. Second, resolution of HSQC peaks to residues in the C-terminal zinc finger following ARE binding (*28*) supports RNA substrate-dependent stabilization of a single or small population of related peptide structures. Finally, thermodynamic characterization of TTP73 binding to high-affinity ARE substrates indicated a significant negative change in heat capacity accompanying peptide−RNA complex formation. This change in heat capacity was manifested as an enhanced entropic penalty for cognate ARE ligand binding relative to noncanonical RNA substrates but was compensated by improved binding enthalpy when an upstream UAUU motif was available for association with the C-terminal zinc finger domain (*26*). Taken together, the structural resistance to denaturant, resolution of HSQC peaks, and unfavorable changes in entropy associated with TTP73 binding to cognate ARE substrates are consistent with restricted local peptide mobility in the TTP73−ARE complex relative to the unbound TTP73 peptide.

Data from this study support a model for ARE substrate recognition by the TTP RNA-binding domain whereby the $Zn^{2+}$-coordinated zinc fingers exhibit significant local flexibility in the absence of an ARE ligand, particularly within the C-terminal finger. It remains possible that such conformational sampling may be less pronounced in the full-length protein, where structural restraints from flanking protein sequences may limit the conformational heterogeneity of the zinc finger domain. Binding to a cognate ARE substrate is associated with stabilization of a unique or small population of folded states within each zinc finger, consistent with induced-fit or selected-fit models of macromolecular complex formation (*29*, *30*). Characteristics of these stabilized folded states include residue side chain burial (denoted by decreased fluorescence quantum yield and collisional quenching constants) at sites distal to the RNA-binding interface (this study) and improved binding potential for cognate RNA substrates, reflected in increased enthalpy of binding (*26*). Furthermore, these studies establish the potential of TTP73 site-directed Trp mutants as powerful tools for forthcoming structural and energetic investigations of RNA recognition by this tandem zinc finger domain. For example, can RNA-dependent folding of the C-terminal zinc finger occur independently of the folded N-terminal zinc finger? Can tandem N-terminal (or C-terminal) zinc finger domains convey RNA-binding affinity and specificity comparable to those of the wild-type peptide? Finally, is adaptive RNA recognition by the wild-type TTP tandem zinc finger domain obligate for the mRNA-destabilizing activity of this protein? We anticipate that future studies including analyses of additional site-specific Trp mutants of the TTP73 peptide will permit resolution of these questions.

## ACKNOWLEDGMENT

We thank Dr. Kristen Varney for assistance with the molecular modeling of the TIS11d−RNA complex.

## REFERENCES

1. Guhaniyogi, J., and Brewer, G. (2001) Regulation of mRNA stability in mammalian cells, *Gene 265*, 11−23.
2. Hargrove, J. L., and Schmidt, F. H. (1989) The role of mRNA and protein stability in gene expression, *FASEB J. 3*, 2360−2370.
3. Chen, C.-Y. A., and Shyu, A.-B. (1995) AU-rich elements: characterization and importance in mRNA degradation, *Trends Biochem. Sci. 20*, 465−470.
4. Bakheet, T., Williams, B. R. G., and Khabar, K. S. A. (2006) ARED 3.0: the large and diverse AU-rich transcriptome, *Nucleic Acids Res. 34*, D111−D114.
5. Barreau, C., Paillard, L., and Osborne, H. B. (2005) AU-rich elements and associated factors: are there unifying principles?, *Nucleic Acids Res. 33*, 7138−7150.
6. Shabalina, S. A., Ogurtsov, A. Y., Lipman, D. J., and Kondrashov, A. S. (2003) Patterns in interspecies similarity correlate with nucleotide composition in mammalian 3′ UTRs, *Nucleic Acids Res. 31*, 5433−5439.
7. Tholanikunnel, B. G., Raymond, J. R., and Malbon, C. C. (1999) Analysis of the AU-rich elements in the 3′-untranslated region of $\beta_2$-adrenergic receptor mRNA by mutagenesis and identification of the homologous AU-rich region from different species, *Biochemistry 38*, 15564−15572.
8. Fialcowitz, E. J., Brewer, B. Y., Keenan, B. P., and Wilson, G. M. (2005) A hairpin-like structure within an AU-rich mRNA-destabilizing element regulates *trans*-factor binding selectivity and mRNA decay kinetics, *J. Biol. Chem. 280*, 22406−22417.
9. Xu, N., Chen, C.-Y. A., and Shyu, A.-B. (1997) Modulation of the fate of cytoplasmic mRNA by AU-rich elements: key

sequence features controlling mRNA deadenylation and decay, *Mol. Cell. Biol. 17*, 4611−4621.
10. Lai, W. S., Carrick, D. M., and Blackshear, P. J. (2005) Influence of nonameric AU-rich tristetraprolin-binding sites on mRNA deadenylation and turnover, *J. Biol. Chem. 280*, 34365−34377.
11. Lykke-Andersen, J., and Wagner, E. (2005) Recruitment and activation of mRNA decay enzymes by two ARE-mediated decay activation domains in the proteins TTP and BRF-1, *Genes Dev. 19*, 351−361.
12. Brewer, G. (1999) Evidence for a 3′-5′ decay pathway for c-*myc* mRNA in mammalian cells, *J. Biol. Chem. 274*, 16174−16179.
13. Chen, C.-Y., Gherzi, R., Ong, S.-E., Chan, E. L., Raijmakers, R., Pruijn, G. J. M., Stoecklin, G., Moroni, C., Mann, M., and Karin, M. (2001) AU binding proteins recruit the exosome to degrade ARE-containing mRNAs, *Cell 107*, 451−464.
14. Tran, H., Schilling, M., Wirbelauer, C., Hess, D., and Nagamine, Y. (2004) Facilitation of mRNA deadenylation and decay by the exosome-bound, DExH protein RHAU, *Mol. Cell 13*, 101−111.
15. Stoecklin, G., Mayo, T., and Anderson, P. (2006) ARE-mRNA degradation requires the 5′-3′ decay pathway, *EMBO Rep. 7*, 72−77.
16. Gao, M., Wilusz, C. J., Peltz, S. W., and Wilusz, J. (2001) A novel mRNA-decapping activity in HeLa cytoplasmic extracts is regulated by AU-rich elements, *EMBO J. 20*, 1134−1143.
17. Wilson, G. M., and Brewer, G. (1999) The search for trans-acting factors controlling messenger RNA decay, *Prog. Nucleic Acid Res. Mol. Biol. 62*, 257−291.
18. Zhang, T., Kruys, V., Huez, G., and Gueydan, C. (2002) AU-rich element-mediated translational control: complexity and multiple activities of trans-acting factors, *Biochem. Soc. Trans. 30*, 952−958.
19. Jing, Q., Huang, S., Guth, S., Zarubin, T., Motoyama, A., Chen, J., Di Padova, F., Lin, S.-C., Gram, H., and Han, J. (2005) Involvement of microRNA in AU-rich element-mediated mRNA instability, *Cell 120*, 623−634.
20. Blackshear, P. J. (2002) mRNA degradation: an important process in controlling gene expression, *Biochem. Soc. Trans. 30*, 945−952.
21. Lai, W. S., Carballo, E., Strum, J. R., Kennington, E. A., Phillips, R. S., and Blackshear, P. J. (1999) Evidence that tristetraprolin binds to AU-rich elements and promotes the deadenylation and destabilization of tumor necrosis factor alpha mRNA, *Mol. Cell. Biol. 19*, 4311−4323.
22. Fenger-Grøn, M., Fillman, C., Norrild, B., and Lykke-Andersen, J. (2005) Multiple processing body factors and the ARE binding protein TTP activate mRNA decapping, *Mol. Cell 20*, 905−915.
23. Lopez de Silanes, I., Zhan, M., Lal, A., Yang, X., and Gorospe, M. (2004) Identification of a target RNA motif for RNA-binding protein HuR, *Proc. Natl. Acad. Sci. U.S.A. 101*, 2987−2992.
24. Wilson, G. M., Sun, Y., Lu, H., and Brewer, G. (1999) Assembly of AUF1 oligomers on U-rich RNA targets by sequential dimer association, *J. Biol. Chem. 274*, 33374−33381.
25. Raghavan, A., Robison, R. L., McNabb, J., Miller, C. R., Williams, D. A., and Bohjanen, P. R. (2001) HuA and tristetraprolin are induced following T cell activation and display distinct but overlapping RNA binding specificities, *J. Biol. Chem. 276*, 47958−47965.
26. Brewer, B. Y., Malicka, J., Blackshear, P. J., and Wilson, G. M. (2004) RNA sequence elements required for high affinity binding by the zinc finger domain of tristetraprolin: Conformational changes coupled to the bipartite nature of AU-rich mRNA-destabilizing motifs, *J. Biol. Chem. 279*, 27870−27877.
27. Worthington, M. T., Pelo, J. W., Sachedina, M. A., Applegate, J. L., Arseneau, K. O., and Pizarro, T. T. (2002) RNA binding properties of the AU-rich element-binding recombinant Nup475/TIS11/Tristetraprolin protein, *J. Biol. Chem. 277*, 48558−48564.
28. Blackshear, P. J., Lai, W. S., Kennington, E. A., Brewer, G., Wilson, G. M., Guan, X., and Zhou, P. (2003) Characteristics of the interaction of a synthetic human tristetraprolin tandem zinc finger peptide with AU-rich element-containing RNA substrates, *J. Biol. Chem. 278*, 19947−19955.
29. Williamson, J. R. (2000) Induced fit in RNA-protein recognition, *Nat. Struct. Biol. 7*, 834−837.
30. Wang, C., Karpowich, N., Hunt, J. F., Rance, M., and Palmer, A. G. (2004) Dynamics of ATP-binding cassette contribute to allosteric control, nucleotide binding and energy transduction in ABC transporters, *J. Mol. Biol. 342*, 525−537.
31. Hudson, B. D., Martinez-Yamout, M. A., Dyson, H. J., and Wright, P. E. (2004) Recognition of the mRNA AU-rich element by the zinc finger domain of TIS11d, *Nat. Struct. Mol. Biol. 11*, 257−264.
32. Spolar, R. S., and Record, M. T., Jr. (1994) Coupling of local folding to site-specific binding of proteins to DNA, *Science 263*, 777−784.
33. Lakowicz, J. R. (1999) *Principles of Fluorescence Spectroscopy*, Kluwer Academic/Plenum, New York.
34. Lai, W. S., Kennington, E. A., and Blackshear, P. J. (2002) Interactions of CCCH zinc finger proteins with mRNA: Non-binding tristetraprolin mutants exert an inhibitory effect on degradation of AU-rich element-containing mRNAs, *J. Biol. Chem. 277*, 9606−9613.
35. Wilson, G. M., Sutphen, K., Moutafis, M., Sinha, S., and Brewer, G. (2001) Structural remodeling of an A+U-rich RNA element by cation or AUF1 binding, *J. Biol. Chem. 276*, 38400−38409.
36. Heyduk, T., Ma, Y., Tang, H., and Ebright, R. H. (1996) Fluorescence anisotropy: rapid, quantitative assay for protein-DNA and protein-protein interaction, *Methods Enzymol. 274*, 492−503.
37. Otto, M. R., Lillo, M. P., and Beechem, J. (1994) Resolution of multiphasic reactions by the combination of fluorescence total-intensity and anisotropy stopped-flow kinetic experiments, *Biophys. J. 67*, 2511−2521.
38. Jameson, D. M., and Sawyer, W. H. (1995) Fluorescence anisotropy applied to biomolecular interactions, *Methods Enzymol. 246*, 283−300.
39. Zelent, B., Kusba, J., Gryczynski, I., Johnson, M. L., and Lakowicz, J. R. (1998) Time-resolved and steady-state fluorescence quenching of *N*-acetyl-L-tryptophanamide by acrylamide and iodide, *Biophys. Chem. 73*, 53−75.
40. Santoro, M. M., and Bolen, D. W. (1988) Unfolding free energy changes determined by the linear extrapolation method. 1. Unfolding of phenylmethanesulfonyl α-chymotrypsin using different denaturants, *Biochemistry 27*, 8063−8068.
41. Manyusa, S., and Whitford, D. (1999) Defining folding and unfolding reactions of apocytochrome $b_5$ using equilibrium and kinetic fluorescence measurements, *Biochemistry 38*, 9533−9540.
42. Salamanca, S., and Chang, J.-Y. (2005) Unfolding and refolding pathways of a major kinetic trap in the oxidative folding of α-lactalbumin, *Biochemistry 44*, 744−750.
43. Sheshadri, S., Lingaraju, G. M., and Varadarajan, R. (1999) Denaturant mediated unfolding of both native and molten globule states of maltose binding protein are accompanied by large $\Delta C_p$'s, *Protein Sci. 8*, 1689−1695.
44. Amann, B. T., Worthington, M. T., and Berg, J. M. (2003) A $Cys_3His$ zinc-binding domain from Nup475/tristetraprolin: A novel fold with a disklike structure, *Biochemistry 42*, 217−221.
45. Michel, S. L. J., Guerrerio, A. L., and Berg, J. M. (2003) Selective RNA binding by a single CCCH zinc-binding domain from Nup475 (tristetraprolin), *Biochemistry 42*, 4626−4630.
46. Worthington, M. T., Amann, B. T., Nathans, D., and Berg, J. M. (1996) Metal binding properties and secondary structure of the zinc-binding domain of Nup475, *Proc. Natl. Acad. Sci. U.S.A. 93*, 13754−13759.
47. Chen, Y., and Barkley, M. D. (1998) Toward understanding tryptophan fluorescence in proteins, *Biochemistry 37*, 9976−9982.

BI061320J